

Anomalous W boson production at HERA

M.N.Dubinin

Institute of Nuclear Physics, Moscow State University

119899 Moscow, Russia

H.S.Song

Center for Theoretical Physics, Seoul National University

Seoul, 151-742, Korea

Abstract

We present the results of complete tree level calculation for W boson production processes $e^-p \rightarrow e^-\mu^+\nu_\mu X$ and $e^-p \rightarrow e^-\mu^-\bar{\nu}_\mu X$ introducing anomalous $WW\gamma$ and WWZ couplings. Detailed results for the distributions of final state particles are obtained. In the region of small momentum transfer we calculate the contribution of hadronlike photon component in the structure function approach.

1 Introduction

In recent years the charged and neutral current sectors of the Standard Model have been tested with excellent precision in the experiments at LEP and SLC. However the gauge boson sector still remains practically untouched by direct measurements of high accuracy. Deviations of three and four gauge boson couplings from the Standard Model values would be an obvious signal of some new physics.

At present time the best limits on anomalous three vector boson couplings are given by CDF and D0 data (Fermilab Tevatron, $\sqrt{s} = 1.8$ TeV) [1]. From the measurement of $W\gamma$ and WW production these collaborations set the limits of order 1 on the deviations of (k, λ) couplings (see section 2.1) from the Standard Model values. Significant improvement of these limits (one order of magnitude) will be achieved by the detection of WW production at LEP2 [2].

In this paper we consider the possibilities of HERA ep collider (30 GeV electrons on 820 GeV protons, $\sqrt{s} = 314$ GeV) for the measurement of the vector boson anomalous couplings. The main difference between our study and the

previous investigations is the exact calculation of tree level amplitude for complete set of diagrams with the four particle final state, including nonstandard $WW\gamma$ and WWZ vertices. At present time the luminosity of HERA (several $pb^{-1}/year$) is too small to produce sufficient number of W bosons. However, after the luminosity upgrade to 100 - 200 pb^{-1} the detection of anomalous signal or setting new limits on the anomalous couplings becomes realistic.

2 The reactions $e^-p \rightarrow e^-\mu^+\nu_\mu X, e^-\mu^-\bar{\nu}_\mu X$

It is known from the previous study (in particular we would like to distinguish the paper [3]) that in the Standard Model W -bosons are produced in ep scattering mainly in the channels $ep \rightarrow eWX$. The contribution of the channel with neutrino in the final state $ep \rightarrow \nu_e W^- X$ is 20 times smaller. The following decay of W boson to muon and muonic neutrino produces the four-fermion state $e^-\mu\nu_\mu q$, and the corresponding event signature is muon(antimuon) with missing transverse momentum. The signal of W boson production in leptonic channels can be observed easier than in hadronic W decay channels, where large QCD background processes must be carefully separated from the signal.

Ten Feynman diagrams for the reaction $e^-q_1 \rightarrow e^-\mu^+\nu_\mu q_2$ are shown in Fig.1. All diagrams have intermediate W and the properties of final state are defined by W interaction dynamics. In this sense all diagrams are ' W^+ producing' and there are no irreducible background graphs that could be neglected in order to simplify the procedure. If we replace diagram 5 by similar one where W^- boson is radiated from the initial electron and change $\mu^+\nu_\mu$ to $\mu^-\bar{\nu}_\mu$, $q_{1,2} \rightarrow \bar{q}_{1,2}$, we obtain a set of ten diagrams for the process $e^-p \rightarrow e^-\mu^-\bar{\nu}_\mu X$ which is ' W^- producing'. Diagrams 4 and 10 in both cases contain $WW\gamma$ and WWZ vertices and in the following we shall use for them nonstandard gauge invariant structure.

If we separate subsets of diagrams from the complete tree level set in Fig.1 and then separate Feynman subgraphs from these subsets, we obtain some approximations that were used in the previous calculations of W production processes. The simplest approximation is given by diagrams 2,3,4 where t -channel photon and s -channel W are taken on-shell ($\gamma^*q_1 \rightarrow W^*q_2$, $2 \rightarrow 2$ subprocess approximation). If we integrate then with equivalent photon structure function for incoming γ^* and consider the decay of on-shell W to $\mu\nu_\mu$, rather satisfactory estimate of total cross section can be obtained. The calculation in $\gamma^*q_1 \rightarrow W^*q_2$ subprocess approximation with anomalous vector boson couplings can be found in [4]. Weak correction to this result is given by diagrams 8,9,10 (containing subprocess $Z^*q_1 \rightarrow W^+q_2$). In the case if the accuracy of equiva-

lent photon approximation is not sufficient, at the next step one could consider $e^- q_1 \rightarrow e^- W^+ q_2$, i.e. $2 \rightarrow 3$ process approximation with on-shell vector boson. Complete tree level calculation for the process $e^- q_1 \rightarrow e^- W^+ q_2$ by means of helicity amplitude method was performed in [5]. If we take the amplitude with W off-shell decaying to fermionic pair (for instance, $e^- q_1 \rightarrow e^- \mu^+ \nu_\mu q_2$ in the $2 \rightarrow 4$ process approximation), the subset of diagrams (2,3,4,5,8,9,10) becomes gauge noninvariant and in order to restore the gauge invariance it is necessary to add ladder diagrams 1,6,7. In the papers [3, 6] complete tree level calculation was performed for the case of Standard Model. We generalize these calculations in the case of complete tree level $2 \rightarrow 4$ muonic channels with anomalous C and P conserving three vector boson couplings, and compare some of our results with [7] where similar analysis was done by means of EPVEC generator [3].

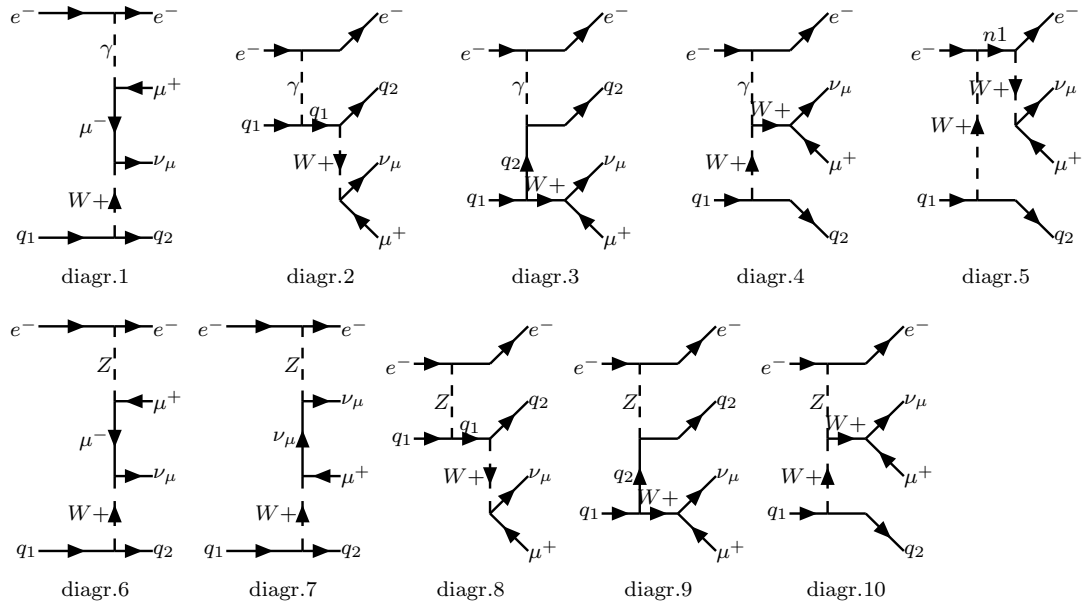


Figure 1: Feynman diagrams for the process $e^- q_1 \rightarrow e^- \mu^+ \nu_\mu q_2$

While the results for total rate provided by $2 \rightarrow 2$ and $2 \rightarrow 3$ approximations can be quite satisfactory, it is not possible to calculate precisely most of the distributions of experimental interest. The accuracy of equivalent photon approximation becomes rather poor (see section 4) especially at large transverse momenta and the narrow-width approximation for the W is usually not good near the W production threshold. At the same time it is obviously difficult to make any conclusions about the origin of new phenomena observing only the deviation of event counting rate from the Standard Model value. It is important

to know what regions of phase space are affected by new interaction dynamics and what is the ratio new signal/ background, i.e. to calculate precisely the distributions of particles in the final state.

Largest contribution to the cross section of $e^- q_1 \rightarrow e^- \mu^+ \nu_\mu q_2$ process is given by diagram 3 when photon and t-channel quark are close to mass shell [8]. In this configuration QCD corrections become large and t -channel intermediate quark can appear nonperturbatively as a constituent of photon ('resolved photon' contribution) when it is usually described by experimentally measured gamma structure function. The process of W production in this picture is quark-antiquark $q_\gamma q_p$ fusion to W when photon fragments into quark constituents q_γ before interacting with the proton constituent quark q_p . It was shown in [3],[8] that resolved photon mechanism is not dominant, but nevertheless the region of small t requires special consideration and careful separation of 'resolved' and ordinary contributions is needed. To be sure that the numbers are not changed significantly by the new parametrizations of γ and p structure functions, we repeat the cross section calculation of the resolved part using the scheme similar to one proposed in [4].

2.1 Anomalous three vector boson couplings

General effective lagrangian of two charged and one neutral gauge boson interaction was proposed in [9]. The restrictions on the lagrangian imposed by invariance under discrete symmetries and gauge invariance were considered in [10]. U(1) gauge invariant, C and P parity conserving effective lagrangian has the form

$$L_{eff} = g_V (W_{\mu\nu}^+ W^{\mu\nu} - W^{\mu\nu} W_\mu^+ V_\nu + k W_\mu^+ W_\nu V^{\mu\nu} + \frac{\lambda}{m_W^2} W_{\rho\mu}^+ W_\nu^\mu V^{\nu\rho}) \quad (1)$$

where $g_\gamma = e$ and $g_Z = e \cos\vartheta_W / \sin\vartheta_W$, $W_{\mu\nu} = \partial_\mu W_\nu - \partial_\nu W_\mu$, $V_{\mu\nu} = \partial_\mu V_\nu - \partial_\nu V_\mu$. Spatial structure of the fourth term in the lagrangian of dimension six is multiplied by m_W^{-2} factor, so parameters λ and k are dimensionless. In the momentum space if all momenta are incoming ($p_1 + p_2 + p_3 = 0$), we have the following expression for $W^+(p_1)W^-(p_2)V(p_3)$ vertex

$$\begin{aligned} \Gamma_{\mu\nu\rho}(p_1, p_2, p_3) = g_V & [g_{\mu\nu}(p_1 - p_2 - \frac{\lambda}{m_W^2}((p_2 p_3)p_1 - (p_1 p_3)p_2)_\rho \\ & + g_{\mu\rho}(k p_3 - p_1 + \frac{\lambda}{m_W^2}((p_2 p_3)p_1 - (p_1 p_2)p_3)_\nu \end{aligned} \quad (2)$$

$$\begin{aligned}
& + g_{\nu\rho} (p_2 - kp_3 - \frac{\lambda}{m_W^2} ((p_1 p_3) p_2 - (p_1 p_2) p_3)_\mu \\
& + \frac{\lambda}{m_W^2} (p_{2\mu} p_{3\nu} p_{1\rho} - p_{3\mu} p_{1\nu} p_{2\rho})]
\end{aligned}$$

In the special case $\lambda = 0$, $k = 1$ this vertex reduces to Standard Model one.

3 Resolved photon contribution

In this section we follow the scheme proposed in [4] for the calculation of resolved photon contribution (diagram 3, Fig.1), but in our case W boson is off-shell and consequently the scale of the equivalent photon approximation is different. Similar procedure (including the corrections from 'finite terms') was considered in [3]. We separate the 'resolved' and 'direct' production mechanisms at the scale $\Lambda^2 = (q_1 - q_W)^2$ (q_1 and q_W are the momenta of initial quark and intermediate W , correspondingly):

$$\sigma = \sigma_{resolved} + \int_{-\Lambda^2}^{-\Lambda^2} \frac{d\sigma_{dir}}{dt} dt \quad (3)$$

Second term in this formula ('direct') is calculated numerically using the exact matrix element for 10 diagrams (see Fig.1) with the transferred momentum cutoff at $t = \Lambda^2$. Resolved photon cross section in the case of monoenergetic initial gamma on shell is given by the convolution of photon structure function (measured in $\gamma\gamma$ collisions) and $q_\gamma q_p \rightarrow W$ fusion cross section

$$\sigma_{resolved} = \int dx_1 dx_2 f_{q_1/\gamma}(x_1, Q_\gamma^2) \sigma(q_1 \bar{q}_2 \rightarrow W) f_{q_2/p}(x_2, Q_p^2) \quad (4)$$

Q_γ^2 and Q_p^2 are the scales for photon and proton structure functions, correspondingly. Using the Breit-Wigner formula in the approximation of infinitely small W width we get

$$\sigma(q_1 \bar{q}_2 \rightarrow W) = \frac{\pi\sqrt{2}}{3} G_F m_W^2 |V_{12}|^2 \delta(x_1 x_2 s - m_W^2) \quad (5)$$

where V_{12} is the CKM matrix element for charged current $\psi_{q_1} \psi_{q_2}$; here and in the following we are not indicating the sum over possible quark species. The experimentally measured photon structure function $f_{q_1/\gamma}$ includes point-like as well as hadron-like parts. In the leading logarithmic approximation the perturbative (point-like) part of photon structure function can be expressed as

$$f_{q_1/\gamma}^{LO}(x_1, Q_\gamma^2) = \frac{3\alpha e_q^2}{2\pi} [x^2 + (1-x)^2] \log \frac{Q_\gamma^2}{\Lambda^2} \quad (6)$$

where e_q is the quark charge. This part was already taken into account by our calculation for direct contribution in (3). In order to avoid double counting in the contributions from gamma structure function and from direct process it is necessary to subtract the point-like term (6) from $f_{q_1/\gamma}(x_1, Q_\gamma^2)$. This procedure was illustrated explicitly for the more simple example of the reaction $\gamma q_1 \rightarrow V q_2$ ($V = Z, W$) in [4] and it was shown that in the case of Z production indeed the LO counterterm (6) rescales the leading logarithmic structure in the direct part from Λ^2 to Q_γ^2 when $f_{q_1/\gamma}(x_1, Q_\gamma^2)$ is taken at momentum transfer Q_γ^2 . Finally the dependence from Λ^2 is absent in the sum of resolved and direct contributions. Our case is certainly more complicated but double counting can be avoided at least on the leading logarithmic level.

Introducing the usual equivalent photon approximation [11] for gamma in the initial state

$$f_{q/e}(x, Q_\gamma^2, Q_{WW}^2) = \int_x^1 \frac{dy}{y} f_{q_1/\gamma}\left(\frac{x}{y}, Q_\gamma^2\right) f_{\gamma/e}(y, Q_{WW}^2) \quad (7)$$

where

$$df_{\gamma/e}(y, Q_{WW}^2) = \frac{\alpha}{2\pi} \left[\frac{1 + (1-x)^2}{xQ^2} - 2m_e^2 \frac{x}{Q^4} \right] dQ^2 \quad (8)$$

$Q_{min}^2 = m_e^2 x^2 / (1-x)$ and $Q_{max}^2 = Q_{WW}^2$ is defined by some process scale that will be discussed later. After the substitution of (5) and (7) into (4) and subtraction of counterterm (6) we finally get

$$\sigma_{resolved} = \frac{\pi\sqrt{2}}{3} G_F m_W^2 |V_{12}|^2 \int_{m_W^2/s}^1 \int_x^1 \frac{dxdy}{xy} \left[f_{q_1/\gamma}\left(\frac{x_1}{y}, Q_\gamma^2\right) - f_{q_1/\gamma}^{LO}\left(\frac{x_1}{y}, \frac{Q_\gamma^2}{\Lambda^2}\right) \right] f_{\gamma/e}(y, Q_{WW}^2) f_{q_2/p}\left(\frac{m_W^2}{x_1 s}, Q_p^2\right) \quad (9)$$

There are four scales $Q_{WW}^2, Q_\gamma^2, \Lambda^2, Q_p^2$ to be defined in this formula. The Weizsacker-Williams scale Q_{WW}^2 can be chosen equal to Λ^2 . It is easy to justify this choice [3] looking at the distribution $d\sigma/d\log Q_{q_1 W}^2$ (Fig.2) calculated exactly for ten diagrams of $2 \rightarrow 4$ process in Fig.1. The flat part of this distribution corresponds to the cross section behaviour $d\sigma/dt \sim 1/t$ (not $1/t^2$ as it seems at the first sight, double poles are cancelled), and rapidly decreases starting from Λ^2 . We always take proton structure function scale $Q_p^2 = m_W^2$. The values of Q_γ^2, Λ^2 are arbitrary and the final result for the sum of resolved and direct contributions (3) should not depend essentially from the choice of these two scales.

In Table 1 we show the results for resolved photon cross section (9) calculated by means of BASES MC integrator [12], using proton structure functions

			MRS A			CTEQ3m		
Q_{WW}	Q_γ	Λ	DG1	LAC2	GRV L0	DG1	LAC2	GRV L0
0.2	m_W	0.2	-11.6	-4.1	-7.3	-11.9	-4.2	-7.6
0.2	$m_W/10$	0.2	-7.5	2.0	-3.3	-7.6	2.7	-3.1
1.0	m_W	1.0	-5.6	3.3	-0.6	-5.7	4.0	-0.1
1.0	$m_W/10$	1.0	1.7	13.4	6.5	1.7	14.8	7.4
5.0	m_W	5.0	4.3	14.7	9.8	4.4	16.3	11.0
5.0	$m_W/10$	5.0	15.7	29.6	21.2	16.0	32.0	23.1

Table 1: Resolved photon cross section of the process $e^-p \rightarrow e^-\mu^+\nu_\mu X$ in fb (see formula (9)). Different sets of photon and proton structure functions were used.

MRS [13] and CTEQ [14], photon structure functions DG [15], LAC-G [16] and GRV [17]. Last two versions of gamma structure function are improved parametrizations in the framework of the approach [15].

One can see that if proton structure function is measured with rather good accuracy and two parametrizations we are using give similar results (consistent within the one standard deviation error of our MC integration), photon structure function is still poorly known. LAC-G parametrization gives the cross section regularly smaller than the values obtained with the help of DG and GRV parametrizations. We checked that our point obtained with the help of LAC2 and HMRS B structure functions at $Q_\gamma^2 = m_W^2/10$, $\Lambda = 5$ GeV and equal to $\sigma_{resolved} = 22$ fb, is close to the value 24 fb given in [3] at the same parameter values. So the possible correction to our result (9) from the so-called 'finite terms' is around 8%, which is much less than the difference of results obtained by using different photon structure functions. Negative cross section in Table 1 means that at a given scale of Λ strong double counting regime of direct and resolved contributions takes place. In other words, most part of the resolved cross section is already taken into account by the calculation for direct term in (3).

4 Complete tree level calculation and anomalous signal of W in the distributions

4.1 General framework

Complete tree level calculation of 10 diagrams in Fig.1 with anomalous three vector boson couplings (direct process) and the following generation of particle distributions were done by means of CompHEP package [18, 19]. The amplitude corresponding to 55 squared diagrams and interferences between diagrams was calculated symbolically. In order to avoid t -channel poles, masses of electron and quarks were kept nonzero.¹ Equivalent photon approximation was not used. After that symbolic expressions are automatically converted to FORTRAN codes and linked to special program for seven dimensional Monte-Carlo integration over four particle phase space, and adaptive integration package VEGAS [21]. In the process of four particle phase space generation we introduce so-called kinematical regularization of the peaks [22] inherent to the amplitude under consideration. Especially these are t -channel gamma peaks in the $ee\gamma$ vertices of diagrams 1-4 (Fig.1), $\mu\mu\gamma$ vertex of diagram 1 and W -resonance peak in the diagrams with s-channel W -boson.

CompHEP package is a software product in the framework of one of a few general approaches [18, 20] developed in recent time for the analysis of multi-particle exclusive states at new colliders, when hundreds of Feynman diagrams contribute to the amplitude and should be exactly calculated. More details can be found in [19].

In our calculations we used the Breit-Wigner propagator with constant width for the W -boson. Generally speaking, if we have some complete tree level set of diagrams, straightforward replacement of lowest order vector boson propagator by the propagator with finite width violates gauge invariance of the amplitude and can break gauge cancellations between diagrams, leading to numerically unstable false results. For this reason we used the well-known "overall" form of propagator replacement [3] when the entire amplitude is multiplied by a factor

$$\frac{p_W^2 - m_W^2}{p_W^2 - m_W^2 + im_W\Gamma_W} \quad (10)$$

Generally speaking in other cases this prescription could affect strongly nonresonant terms in the amplitude [23] (in the region of phase space where $p^2 \sim m_W^2$),

¹For this reason we need Λ cut only for matching of direct and resolved parts of cross section. For instance, if $m_u = 5$ MeV, $m_d = 10$ MeV, $m_s = 0.2$ GeV and $m_c = 1.3$ GeV and there are no kinematical cuts, $\sigma_{dir}(ep \rightarrow e\mu^+\nu_\mu X) = 102.5(5)$ fb in the standard case with MRS A structure functions.

but the case under consideration is free from this difficulty.

$\Lambda = 0.2 \text{ GeV}$						
λ	k	$eu \rightarrow e\mu^+\nu_\mu d$	$ed \rightarrow e\mu^+\nu_\mu \bar{u}$	$eu \rightarrow e\mu^+\nu_\mu s$	$e\bar{s} \rightarrow e\mu^+\nu_\mu \bar{c}$	σ_{tot}
0	1	68.2(4)	15.2(1)	3.5(0)	5.2(0)	92.1(5)
1	1	72.6(5)	15.6(1)	3.7(0)	5.3(0)	97.2(6)
0	0	52.6(5)	13.6(1)	2.7(0)	4.6(0)	73.5(6)
0	2	99.6(6)	17.2(2)	5.1(0)	6.3(0)	128.2(8)
$\Lambda = 1.0 \text{ GeV}$						
0	1	61.2(4)	12.4(2)	3.1(0)	5.2(0)	81.9(6)
1	1	66.0(4)	12.6(1)	3.4(0)	5.3(0)	87.3(5)
0	0	45.3(3)	10.8(1)	2.3(0)	4.6(0)	63.0(4)
0	2	92.7(6)	14.9(1)	4.8(0)	6.3(0)	118.7(7)
$\Lambda = 5.0 \text{ GeV}$						
0	1	52.5(3)	8.9(0)	2.7(0)	4.5(0)	68.6(3)
1	1	57.4(4)	9.0(0)	2.9(0)	4.6(0)	73.9(4)
0	0	36.4(3)	7.4(0)	1.9(0)	3.9(0)	49.6(3)
0	2	83.8(5)	11.1(0)	4.3(0)	5.6(0)	104.8(5)

Table 2: Total cross sections (fb) of the main partonic W^+ producing processes (see 10 diagrams in Fig.1) in the reaction $e^-p \rightarrow e^-\mu^+\nu_\mu X$ for the various sets of k , λ . Invariant kinematical cut $\Lambda^2 = (p_q - p_W)^2$. Proton structure function MRS A. One standard deviation error of Monte-Carlo integration for the last digit is indicated in brackets.

The accuracy of our Monte Carlo calculation of σ_{dir} is usually 0.6-0.8% (see Table 2). This choice is related to the precision of proton structure function parametrization. We checked that if we replace the proton structure set MRS A [13] that we are using by the set CTEQ3m [14], the relative difference of results obtained with these two sets does not exceed 1%.

Four partonic processes from 12 possible give the main contribution to W boson production. We present the results of total cross section calculation for the main subprocesses of the W^+ production channel $e^-p \rightarrow e^-\mu^+\nu_\mu X$ in Table 2. Main contribution comes from the subprocess $e^-u \rightarrow e^-\mu^+\nu_\mu d$. The remaining 8 partonic reactions have very small individual total cross sections and the sum of their contributions is of order 1 fb . The cross section of W^- production channel $e^-p \rightarrow e^-\mu^-\bar{\nu}_\mu X$ is compared with the case of W^+ production in Table 4. In the case of W^- production the main partonic subprocess is $e^-d \rightarrow e^-\mu^+\nu_\mu u$ and the total rate is slightly smaller because there are less d -

$\Lambda = 0.2 \text{ GeV}, E_\mu > 10 \text{ GeV, missing } p_T > 20 \text{ GeV}$						
λ	k	$eu \rightarrow e\mu^+\nu_\mu d$	$ed \rightarrow e\mu^+\nu_\mu \bar{u}$	$eu \rightarrow e\mu^+\nu_\mu s$	$e\bar{s} \rightarrow e\mu^+\nu_\mu \bar{c}$	σ_{tot}
0	1	49.2(4)	11.1(1)	2.5(0)	3.6(0)	66.4(5)
1	1	54.7(5)	11.4(1)	2.8(0)	3.7(0)	72.6(6)
0	0	36.6(4)	9.8(1)	1.8(0)	3.0(0)	51.2(5)
0	2	75.9(5)	12.8(2)	3.9(0)	4.5(0)	97.1(7)

Table 3: The same as in Table 2 with the kinematical cuts imposed $E_\mu > 10 \text{ GeV}$, missing $p_T > 20 \text{ GeV}$. These cuts are used to exclude the misidentification backgrounds in the electron channel (see section 4.2).

quarks in the proton than u -quarks. Resolved photon contribution from Table 1 is also indicated. One can see that indeed rather weak dependence of $\sigma_{dir} + \sigma_{res}$ from the cutoff Λ takes place in so far as the decrease of direct part with the growth of Λ is compensated by the increase of resolved part.

We already mentioned in Section 3 that $Q_p^2 = m_W^2$ was always taken as the momentum transferred scale in the proton structure functions. It is important to find out how the changes of Q_p^2 affect the total cross section value and compare the possible deviation of total rate caused by the change of hadronic scale with the deviation of total rate coming from anomalous three vector boson couplings. The uncertainties coming from the value of Q_p^2 should be less than the effect of anomalous couplings to make the phenomenological restrictions based on the value of total rate more meaningful. We show the numbers for total cross section of the main W^+ producing partonic process $eu \rightarrow e\mu\nu_\mu d$ calculated for proton structure function scales $m_W^2/2$ and $2m_W^2$ in Table 5. These values are taken as illustrative ones because in real partonic processes the contributions from so small/large values of Q_p^2 are negligible. We can see that the total cross section deviation from the standard choice of hadronic scale $Q_p^2 = m_W^2$ is around 2.5 - 3%, while the effects of anomalous W couplings are much larger. For instance, the effect coming from anomalous k -term in 20 - 30% and the effect of anomalous λ term is 6 - 8% (Table 2).

4.2 The reactions $e^-p \rightarrow e^-e^+\nu_e X$, $e^-p \rightarrow e^-e^-\bar{\nu}_e X$ and the comparison with EPVEC generator

Total number of diagrams in the channels $e^-p \rightarrow e^-e^+\nu_e X$ and $e^-p \rightarrow e^-e^-\bar{\nu}_e X$ is 20 (ten additional diagrams to Fig.1 with t -channel W -boson exchanges appear). However at HERA energy the correction coming from these additional

			Λ		
	λ	k	0.2	1.0	5.0
$\sigma_{dir}(W^+)$	0	1	92.1	81.9	68.6
	1	1	97.2	87.3	73.9
	0	0	73.5	63.0	49.6
	0	2	128.2	118.7	104.8
$\sigma_{res}(W^+)$			-4.1	3.3	14.7
$\sigma_{dir} + \sigma_{res}, W^+, \text{SM}$			88.0	85.2	83.3
$\sigma_{dir}(W^-)$	0	1	80.3	68.6	52.4
	1	1	82.7	70.6	53.9
	0	0	69.5	57.6	41.4
	0	2	97.6	86.0	69.5
$\sigma_{res}(W^-)$			-11.0	-3.8	7.9
$\sigma_{dir} + \sigma_{res}, W^-, \text{SM}$			69.3	64.8	60.3

Table 4: Total cross sections (fb) of the reactions $e^-p \rightarrow e^-\mu^+\nu_\mu X$ (W^+ production) and $e^-p \rightarrow e^-\mu^-\bar{\nu}_\mu X$ (W^- production) in the case of standard (SM) and anomalous three vector boson interaction at different values of Λ cutoff parameter. Proton structure function MRS A. In the calculation of resolved photon contribution gamma structure function LAC-G2 was taken at the scale m_W .

diagrams is very small because they do not contain t -channel photon poles. Usually this weak contribution is neglected. Such approximation was used in the recent simulation for HERA [7] (by means of EPVEC generator [3]), where event topology and realistic kinematical cuts were considered in more details.

The electron channels $e^-e^+\nu_e X$ and $e^-e^-\bar{\nu}_e X$ are more difficult for experimental study than the muon channels $e^-\mu^+\nu_\mu X$ and $e^-\mu^-\bar{\nu}_\mu X$. First, large background from the neutral current deep inelastic scattering process $ep \rightarrow eX$ appears in the case when the final jet energy is not completely registered in the hadronic calorimeter and for this reason some missing p_T is observed. Second, large background from the charged current DIS process $ep \rightarrow \nu X$ appears in the case when π^0 from the final jet is misidentified as $e^-(e^+)$ giving again the final state with $e^-(e^+)$, jet and missing p_T . In order to suppress these misidentification backgrounds the following kinematical cuts were used in [7]: (1) isolated electron with the energy $E_e > 10$ GeV (2) missing transverse momentum $p_T > 20$ GeV are required. The requirement of isolated electromagnetic cluster is removed for the case of muonic channels, and 10 GeV energy cut seems too

strong for the final muon, since good reconstruction of several GeV muons is available in ZEUS and H1 detectors. Missing transverse momentum cut also seems not necessary for the muon channels (scattered lepton is different from W decay lepton).

We checked by direct calculation that in the absence of missing p_T cut, muon energy cut at 2-3 GeV practically does not affect the numbers for total cross sections shown in Table 2 and Table 4. The combination of muon energy cut at 10 GeV and missing p_T cut at 20 GeV gives the cross sections by 30-35% smaller than before cuts (see Table 3). Following [7] we shall consider electron channels in the approximation of 10 diagrams subset (Fig.1) with the kinematical cuts $E_e > 10$ GeV and missing $p_T > 20$ GeV.

In Fig.3 we show the distributions of energy, angle with the beam and transverse momentum for electron, muon and final quark in the muonic channel $e^- \mu^+ \nu_\mu X$, obtained by means of CompHEP (Standard Model case). The same distributions for electron channel, obtained with the help of EPVEC generator, can be found in [7]. (We are using in (3) $\Lambda = 0.2$ GeV, while the distributions in [7] are calculated using $\Lambda = 5$ GeV.) Although the normalization is not indicated in [7], one can observe that the agreement of the shapes is satisfactory. Soft muons in the distributions $d\sigma/dE_\mu$ and $d\sigma/dp_{T\mu}$ come from the ladder diagrams 1,6,7 in Fig.1. Jets at the angle 180 degrees with the proton beam appear from diagram 3, Fig.1, when the quasireal photon produces two quarks collinear to initial electron. Soft muons and backward jets are absent in [7], because besides the E_e and missing p_T cuts mentioned above, the EPVEC generator contains build-in cuts [24] separating some region of phase space near the W pole.

4.3 Sensitivity to anomalous couplings

Let us return to our calculation with anomalous interaction of vector bosons. We can estimate approximately the possibilities of HERA in the detection of anomalous couplings using a simple criteria (see, for instance, [25]) for the number of events N that is necessary to observe $\Delta\sigma$ deviation from the total cross section value σ :

$$\frac{\Delta\sigma}{\sigma} \sim \frac{1}{\sqrt{N}} \quad (11)$$

It follows from Tables 2,4 that at the integrated luminosity of HERA $L = 200 pb^{-1}$ in the channels of W^+ and W^- production $e^- \mu^+ \nu_\mu q$ and $e^- \mu^- \bar{\nu}_\mu q$ we shall have about 35 events/year. Deviation of λ in the vertex (1) from the zero standard value $\Delta\lambda = 1$ gives us 5% deviation in the total W production rate and we need about 400 events to observe it. However the deviation $\Delta k=1$

$(\Delta k = k - 1)$ changes the total cross section by 20-40 % and less than 25 events will be needed for some experimental evidence. W^+ and W^- production in the channels $e^-e^+\nu_e q$ and $e^-e^-\bar{\nu}_e q$ will give slightly less reliably reconstructed events than in muonic channels (kinematical cuts must be introduced to tune off the misidentification backgrounds), so in total around 60 W bosons/year decaying to electrons and muons could be observed. It follows that it will be difficult to improve CDF and D0 limits on λ [1], but some improvement of Δk restriction could be possible.

More precisely, systematic errors on the detector acceptance A and the uncertainty in the luminosity measurement L should be taken into account. The former are estimated on the level of 2%(1%) for the integrated luminosity of order 10^2 pb^{-1} (10^3 pb^{-1}) and the latter is taken to be 2%. The uncertainty of the total cross section measurement has the form [7]

$$\frac{\Delta\sigma}{\sigma} = \left(\frac{1}{N} + \left(\frac{\Delta L}{L} \right)^2 + \left(\frac{\Delta A}{A} \right)^2 \right)^{\frac{1}{2}} \quad (12)$$

The acceptances in both electron and muon channels are taken to be 65%. From equation (12) we derive the following limits for Δk and λ , giving the observable deviation of total cross section from the Standard Model value at 68% and 95% confidence level:

$$\begin{aligned} -1.70 < \lambda < 1.70, \quad & -1.05 < \Delta k < 0.48, & 68\% \text{ CL} \\ -2.24 < \lambda < 2.24, \quad & \Delta k < 0.89, & 95\% \text{ CL} \end{aligned}$$

at the integrated luminosity 200 pb^{-1} , and

$$\begin{aligned} -1.03 < \lambda < 1.03, \quad & -0.31 < \Delta k < 0.27, & 68\% \text{ CL} \\ -1.75 < \lambda < 1.75, \quad & -0.58 < \Delta k < 0.46, & 95\% \text{ CL} \end{aligned}$$

at the integrated luminosity 1000 pb^{-1} . Here only one coupling from the pair (λ, k) is assumed to be different from the SM value. We do not indicate the negative 95% CL Δk limit at the integrated luminosity 200 pb^{-1} because the cross section deviation from the SM value stops to increase starting from $\Delta k \sim -1.5$ and the effect cannot be observed with small statistics. However, positive Δk limit at the same luminosity is competitive with the early expectations from LEP2 [2]. These limits could be of course improved by taking into account the channels $W \rightarrow \text{jets}$ with final electron and three jets in the final state. Low acceptance in the jets channel ($\sim 20\%$, [7]) and complicated situation with the separation of QCD backgrounds requires an independent careful study, and we are not considering this possibility here.

Of course the calculation of total rate is very important and the ratio $\sigma_{tot}(W)/\sigma_{tot}(Z)$ that was considered in [4] could be the clear indicator to anomalous gauge boson coupling. However the only way to see definitely if the deviation of the ratio is really due to anomalous $WW\gamma$ interaction but not caused by some other reason, is to inspect what regions of phase space are affected by anomalous W interaction dynamics and how they are affected. It is natural to use, as proposed in [5], the distributions of final quark and muon transverse momenta.

We show the distributions of final quark jet transverse momentum in Fig.4,5. It follows from symbolic calculation in $2 \rightarrow 2$ approximation that the cross section depends from λ quadratically [4]. We checked at complete tree level $2 \rightarrow 4$ that this is true for σ_{tot} at about 1% accuracy and no difference at positive and negative values of λ is observed in the distributions. The deviation of k is clearly seen (Fig.5), $d\sigma/dp_T$ becomes harder when k is less than standard value $k = 1$.

The distributions of final muon transverse momentum are shown in Fig.6,7. Similar to the previous case of jet p_T distribution, the effect coming from λ is very small and the dependence of distribution from k is rather strong. The forward and backward slopes of W peak can be slightly shifted if we take into account W production by the resolved photon (see the details in [3]), but this shift is the same for standard and nonstandard cases.

The distributions of final muon rapidity for the standard and anomalous cases are shown in Fig.8. The direction of proton beam was chosen as the direction of positive rapidity axis.

An important point concerning the p_T distributions of the quark and muon for the direct process is their sensitivity to higher order QCD corrections, which could be large. As it was stated in [4, 5], the integration close to u -channel pole

		$m_W^2/2$	m_W^2	$2m_W^2$
λ	k			
0	1	70.6(5)	68.2(4)	66.3(6)
1	1	75.5(5)	72.6(5)	71.1(4)
0	0	54.1(4)	52.6(5)	51.2(4)
0	2	102.3(6)	99.6(6)	96.2(6)

Table 5: Total cross section (fb) of the main W^+ producing partonic process $eu \rightarrow e\mu\nu_\mu d$ calculated using three Q^2 scales in the parametrizations of proton structure function MRS A.

λ	k	exact result	$Q_{WWA} = m_W$	$Q_{WWA} = 20 \text{ GeV}$
0	1	61.2(4)	66.6(8)	61.1(5)
1	1	66.0(4)	70.9(6)	64.5(5)
0	0	45.3(3)	49.4(5)	46.5(4)
0	2	92.7(6)	96.7(9)	88.1(8)

Table 6: Comparison of exact calculation (fb) for the process $e^-u \rightarrow e^-\mu^+\nu_\mu d$ with equivalent photon approximation for the process $\gamma u \rightarrow \mu^+\nu_\mu d$ calculated at the scale Q_{WW} (8) equal to m_W and 20 GeV, $\Lambda = 1.0 \text{ GeV}$.

in the diagram 3, Fig.1 involves the momenta of the order Λ_{QCD} in the small p_T region, when the QCD corrections can be expected to be significant. Total cross section in the absence of u -channel or p_T cuts contains some degree of uncertainty. It was mentioned in [5] that in connection with normalization uncertainty of the cross section the events when the jet escapes detection and only the lepton with missing p_T are observed could provide an important test on the normalisation of W production rate.

Finally we would like to discuss the question of equivalent photon approximation [11] accuracy in our case. In Table 6 we compare exact result for the partonic subprocess $eu \rightarrow e\mu^+\nu_\mu d$ and the equivalent gamma approximation calculation for the process $\gamma u \rightarrow \mu^+\nu_\mu d$. In the latter case initial photon momentum is distributed according to (8) where we used two different choices of Q_{WW} . One can see that the 'natural' choice $Q_{WW} = m_W$ overestimates the cross section by 8% (let us remind (see Table 4) that the effect of $\Delta\lambda = 1$ is 5%). It is possible of course to adjust Q_{WW} which is not strictly fixed at any value, but defined by some typical process dependent momentum transferred scale, and get agreement of exact and WW cross sections for the standard case $\lambda = 0$, $k = 1$; it turns out that the corresponding value is $Q_{WW} = 20 \text{ GeV}$. However, after fixing of this value in the anomalous case $\lambda = 0$, $k = 2$ again we observe 5% deviation. Equivalent approximations become too rough if precise separation of the signal is needed.

5 Conclusion

We presented the results of complete tree level calculation for the W boson production processes at the energy of HERA collider, introducing anomalous C and P conserving three vector boson couplings (1). The main W^+ and W^- production channels $e^-p \rightarrow e^-l^+\nu_l X$ and $e^-p \rightarrow e^-l^-\bar{\nu}_l X$ ($l = e, \mu$) were con-

sidered. Following the earlier publications [3, 4] we separated the phase space at some scale of momentum transferred from the constituent quark to W -boson in order to take into account the resolved photon contribution to the total rate. Resolved photon part was calculated in the structure function approach, using new parametrizations of photon and proton distribution functions. Perturbative (direct) part of the cross section was considered by means of CompHEP package [18],[19], when the tree level $2 \rightarrow 4$ amplitude, corresponding to ten diagrams for each of W^+ and W^- production processes, is calculated exactly without any approximations. Some uncertainty in the normalization of total cross section exists for the reason of possibly large QCD corrections in the phase space region near the u -channel quark pole. In the muonic channels under consideration the total cross section is equal approximately to 150-160 fb, giving about 35 events/year at the integrated luminosity 200 pb^{-1} . Kinematical cuts are necessary in the electron channels for separation of misidentification backgrounds, and the number of identifiable events from $W \rightarrow e\nu_e$ is slightly smaller.

We show explicitly what regions of phase space are affected by anomalous three vector boson interaction dynamics. In particular it follows from our analysis that even at the integrated luminosity 1000 pb^{-1} it will be extremely difficult to separate anomalous λ term effect in (1) when $\Delta\lambda$ is less than 1.5 (as already restricted by Tevatron data), but rather easy to observe anomalous k term effect, when Δk is of order 0.4-0.8, which is strongly competitive with LEP2 possibilities.

Acknowledgements

The authors are grateful to Edward Boos, C.S.Kim and Alexander Pukhov for useful discussions. M.D. would like also to thank the Center for Theoretical Physics, Seoul National University, for hospitality. The research of M.D. was partially supported by INTAS grant 93-1180ext and RFBR grant 96-02-19773a.

References

- [1] F.Abe et al., Phys.Rev.Lett. 74 (1995) 1936, 75 (1995) 1018
S.Adachi et al., Phys.Rev.Lett. 75 (1995) 1034, 75 (1995) 1024
- [2] M.Bilenky, J.-L.Kneur, F.M.Renard, D.Schildknecht, Nucl.Phys. B409 (1993) 22
Triple gauge boson couplings, in:*Physics at LEP2*, ed. by G.Altarelli, T.Sjostrand, F.Zwirner, CERN Yellow report 96-01, 1996, vol.I, p.525

F.A.Berends, A.van Sighem, Nucl.Phys. B454 (1995) 467 (hep-ph/9506391)
C.G.Papadopoulos, Phys.Lett. B352 (1995) 144 (hep-ph/9503276)

- [3] U.Baur, J.Vermaseren, D.Zeppenfeld, Nucl.Phys. B375 (1992) 3
- [4] C.S.Kim, Jungil Lee, H.S.Song, Z.Phys. C63 (1994) 673
- [5] U.Baur, D.Zeppenfeld, Nucl.Phys. B325 (1989) 253
- [6] M.Janssen, Z.Phys. C52 (1991) 165
M.Böhm, A.Rosado, Z.Phys. C39 (1988) 275
- [7] V.Noyes, in: *Proc.of the Workshop on Future Physics at HERA 1995/96*,
ed. by G. Ingelman, A. De Roeck and R. Klanner, p.190
- [8] M.Drees, Mod.Phys.Lett., A2 (1987) 573
J.Blümlein, G.Schuler, in: *Proc.of Snowmass Summer Study on Research
Directions for the Decade*, 1990
- [9] K.J.F.Gaemers, G.J.Gounaris, Z.Phys. C1 (1979) 259
- [10] K.Hagiwara, R.D.Peccei, D.Zeppenfeld, K.Hikasa, Nucl.Phys. B282 (1987)
253
- [11] C.F.Weizsäcker, Z.Phys. 88 (1934) 612
E.J.Williams, Phys.Rev. 45 (1934) 729
- [12] S.Kawabata, Comp.Phys.Comm. 41 (1986) 127
- [13] A.D.Martin, W.J.Stirling, R.G.Roberts, Phys.Rev. D51 (1995) 4756
- [14] H.L.Lai, J.Botts, J.Huston, J.G.Morfin, J.F.Owens, J.W.Qiu,
W.K.Tung, H.Weerts, Phys.Rev. D51 (1995) 4763
- [15] M.Drees, K.Grassie, Z.Phys. C28 (1985) 451
- [16] H.Abramowicz, K.Charchula, A.Levy, Phys.Lett. B269 (1991) 458
- [17] M.Gluck, E.Reya, A.Vogt, Phys.Rev. D46 (1992) 1973, Phys.Rev. D45
(1992) 3986
- [18] E.Boos, M.Dubinin, V.Ilyin, A.Pukhov, V.Savrin, preprint INP MSU 94-
36/358, 1994 (hep-ph/9503280)
in: *Proc.of X Workshop on High Energy Physics and Quantum Field Theory*,
ed. by B.Levtchenko, V.Savrin, Moscow, 1996, p.101

- [19] Event generators for WW physics, in: *Physics at LEP2*, ed. by G. Altarelli, T. Sjostrand, F. Zwirner, CERN report 96-01, 1996, vol.II, p.3
- [20] T. Ishikawa, T. Kaneko, K. Kato, S. Kawabata, Y. Shimizu, H. Tanaka, KEK report 92-19, 1993
 F. A. Berends, R. Pittau, R. Kleiss, Nucl. Phys. B424 (1994) 308
 E. Accomando, A. Ballestrero, WPHACT, hep-ph/9607317
 G. Passarino, Comp. Phys. Commun. 97 (1996) 261 (hep-ph/9602302)
- [21] P. Lepage, J. Comput. Phys. 27 (1978) 192; Cornell preprint CLNS-80/447, 1980
- [22] V. Ilyin, A. Kovalenko, A. Pukhov, Int. J. Mod. Phys. C7 (1996) 761 (hep-ph/9612479)
- [23] E. Boos, M. Dubinin, L. Dudko, Int. J. Mod. Phys. A11 (1996) 5015 (hep-ph/9602220)
- [24] U. Baur, private communication
- [25] B. Schrempp, F. Schrempp, N. Wermes, D. Zeppenfeld, Nucl. Phys. B296 (1988) 1

Figures

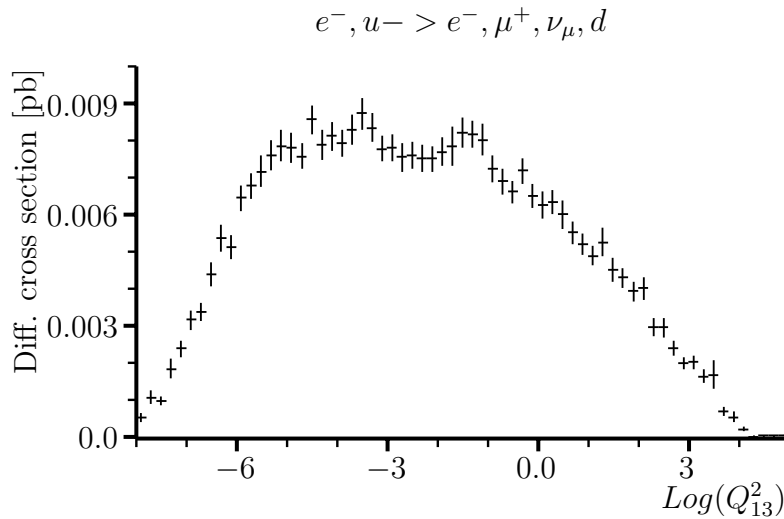


Figure 2: Distribution over logarithm of momentum transferred squared $Q_{13}^2 = t_{13} = (p_e^{in} - p_e^{out})^2$. Flat part of the distribution corresponds to the behaviour $d\sigma/dt \sim 1/t_{13}$

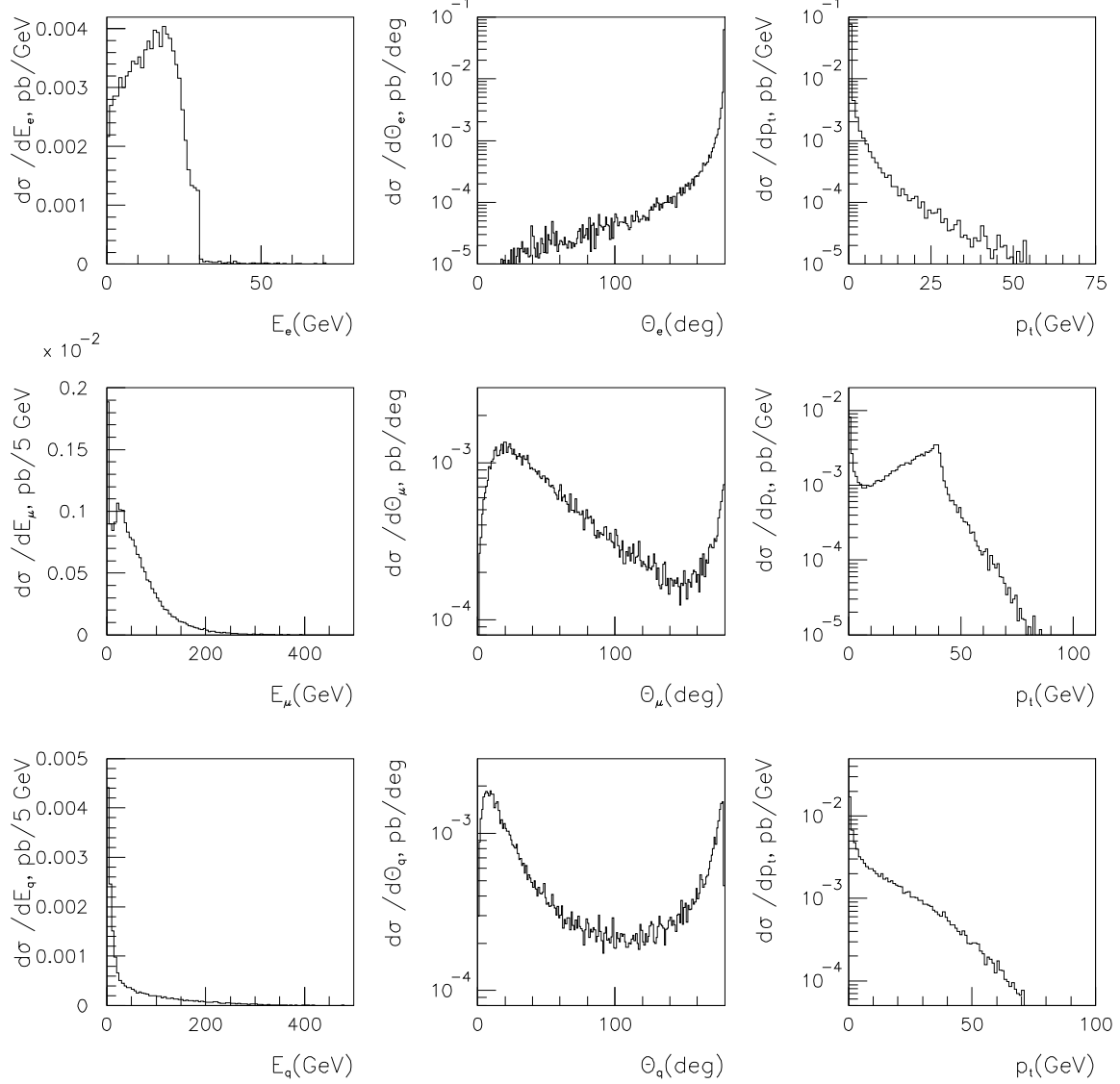
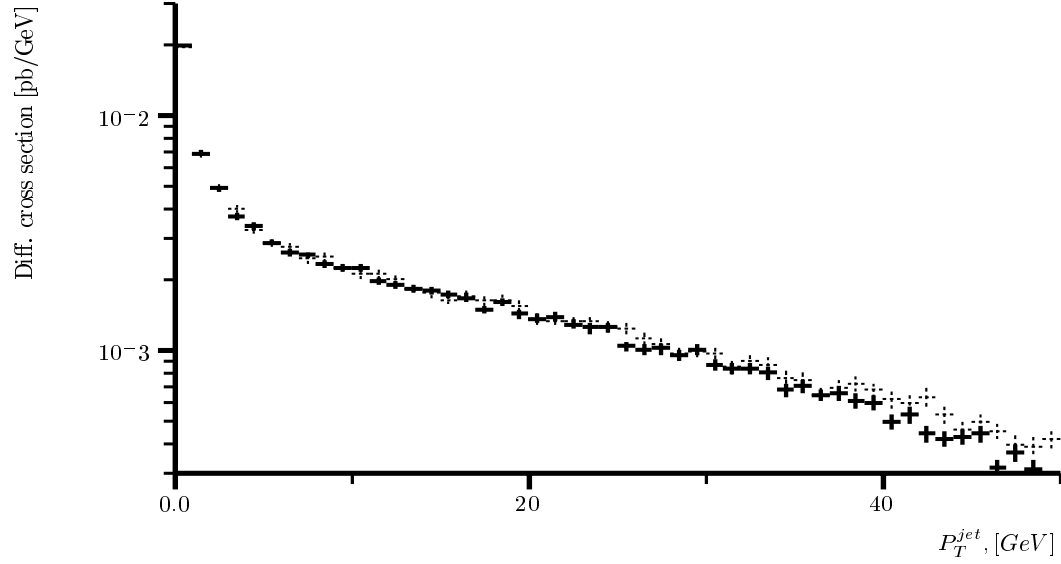


Figure 3: First row of plots - distributions of the electron energy, scattering angle and transverse momentum in the process $e^-p \rightarrow e^-\mu^+\nu_\mu X$. Second row of plots - distributions of the muon energy, muon scattering angle and transverse momentum. Third row of plots - distributions of the quark energy, angle and transverse momentum for the same process. No kinematical cuts, all calculations were done by means of CompHEP [18] ($\Lambda = 0.2$ GeV) to be compared with the same distributions obtained by means of EPVEC generator ($\Lambda = 5.0$ GeV), see [7]

$$e^- p \rightarrow e^- \mu^+ \nu_\mu X$$



$$e^- p \rightarrow e^- \mu^+ \nu_\mu X$$

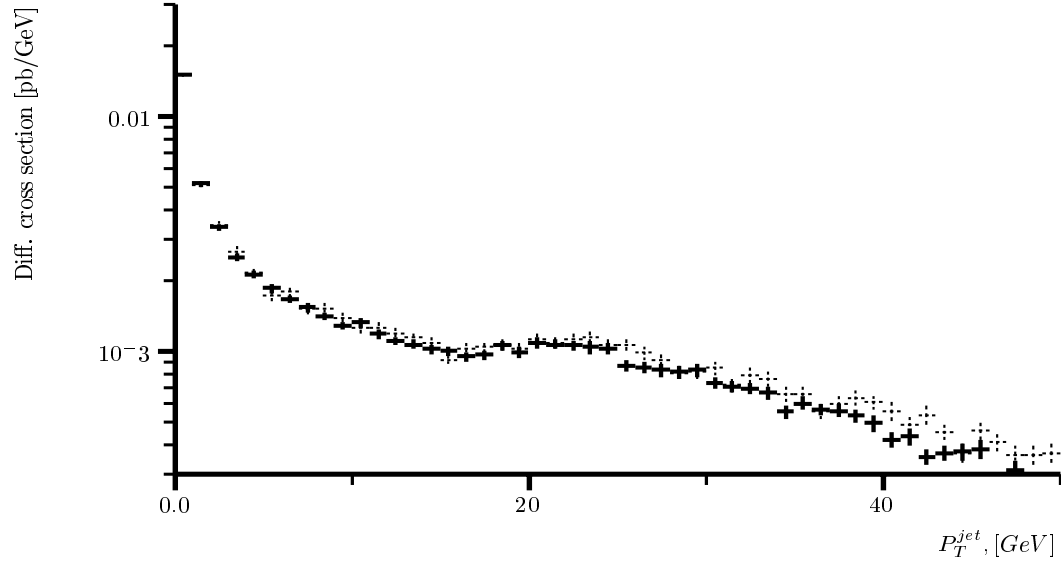
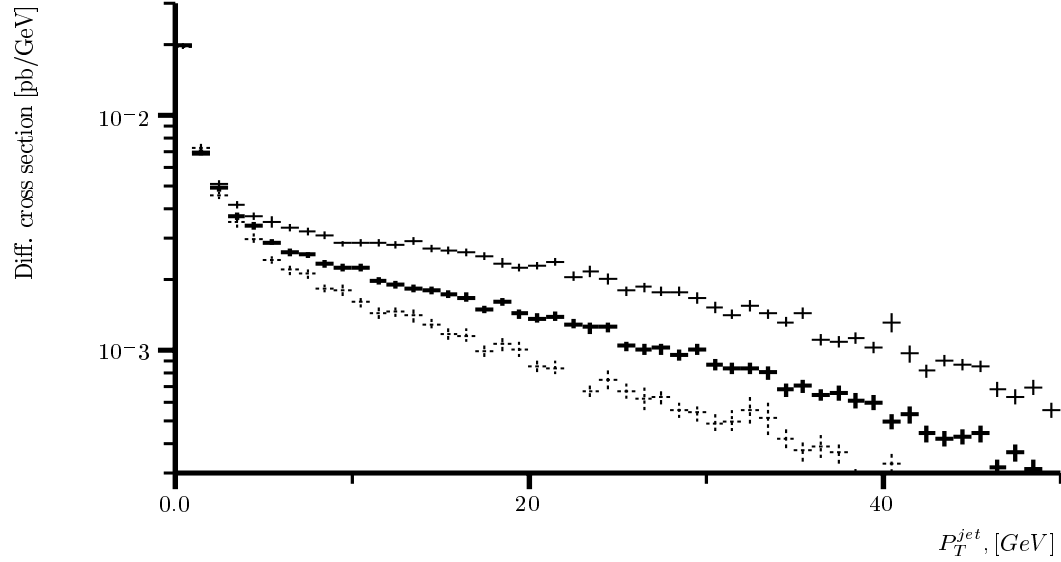


Figure 4: Distribution of jet transverse momentum in the reaction $e^- p \rightarrow e^- \mu^+ \nu_\mu X$. Upper plot: no kinematical cuts, solid lines - standard case, dash lines - anomalous three vector boson couplings case, $\lambda = 1$, $k = 1$ Lower plot: the same distributions after kinematical cuts $E_\mu \geq 10$ GeV, missing $p_T \geq 20$ GeV.

$$e^- p - \rightarrow e^- \mu^+ \nu_\mu X$$



$$ep - \rightarrow e^- \mu^+ \nu_\mu X$$

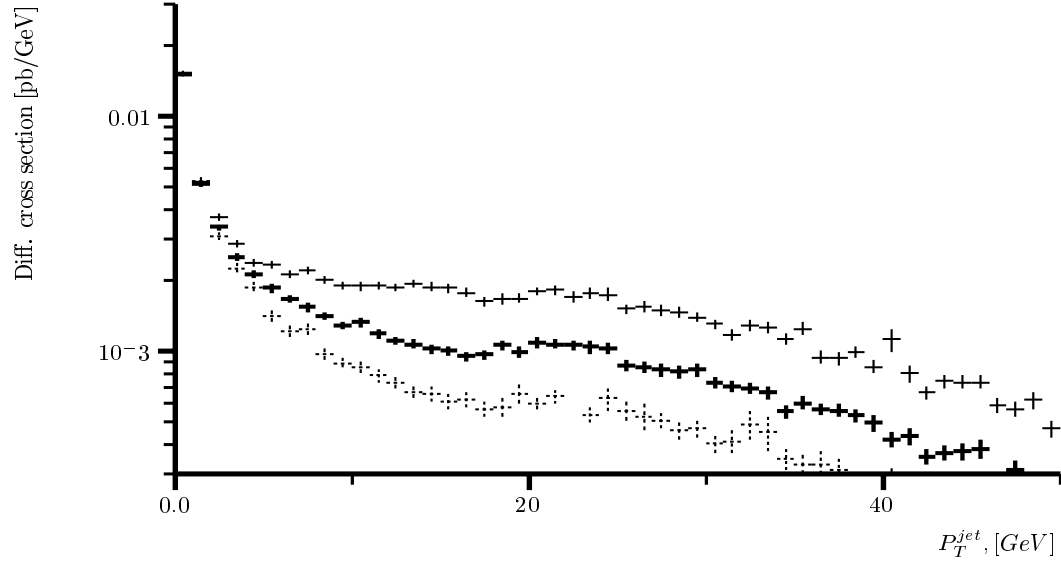


Figure 5: Distribution of jet transverse momentum in the reaction $e^- p \rightarrow e^- \mu^+ \nu_\mu X$. Upper plot: no kinematical cuts, solid lines - standard case, dash lines - anomalous three vector boson couplings case, $\lambda = 0$, $k = 0$, thin solid lines - $\lambda = 0$, $k = 2$. Lower plot: the same distributions after kinematical cuts $E_\mu \geq 10$ GeV, missing $p_T \geq 20$ GeV.

$$e^- p \rightarrow e^- \mu^+ \nu_\mu X$$

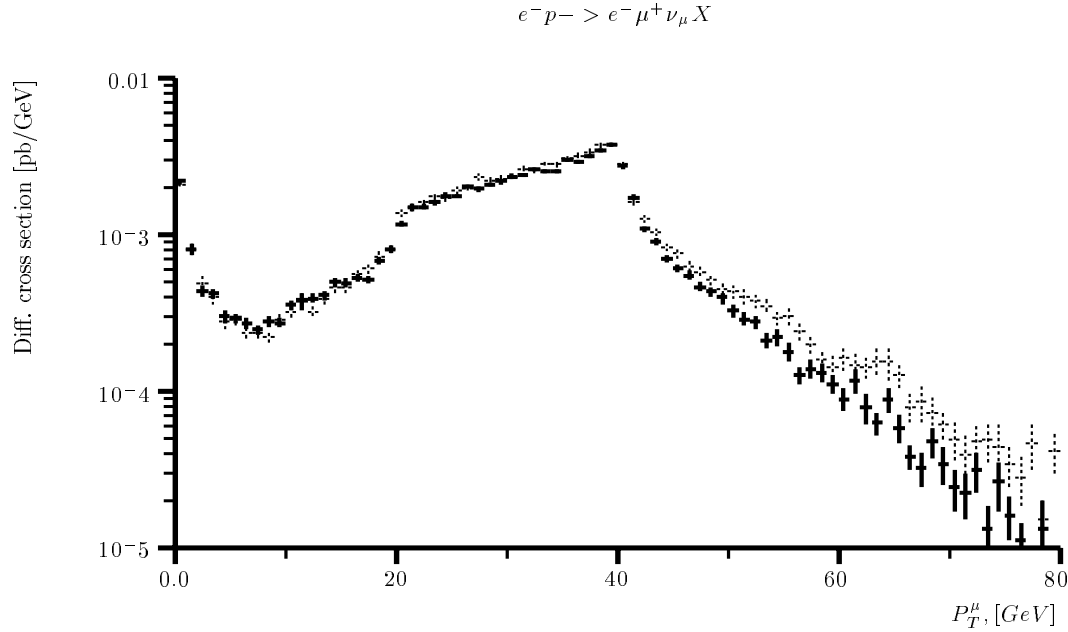
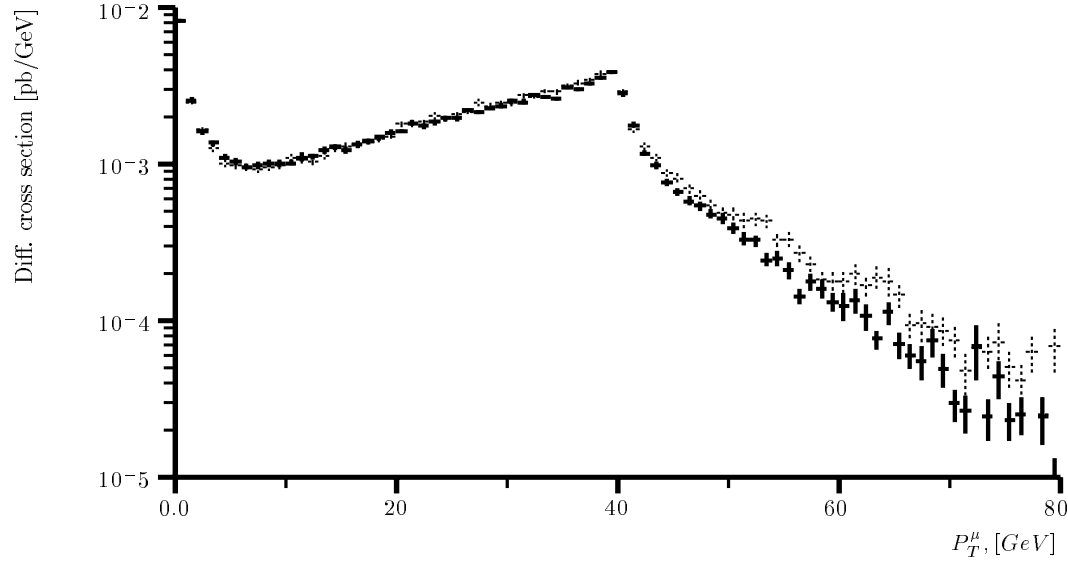
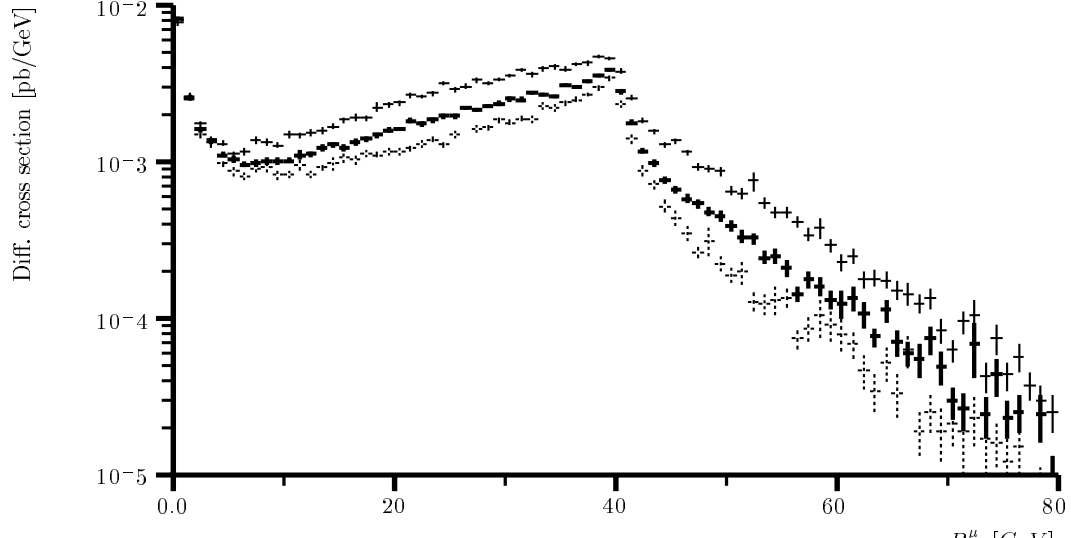


Figure 6: Distribution of muon transverse momentum in the reaction $e^- p \rightarrow e^- \mu^+ \nu_\mu X$. Upper plot: no kinematical cuts, solid lines - standard case, dash lines - anomalous three vector boson couplings case, $\lambda = 1$, $k = 1$ Lower plot: the same distributions after kinematical cuts $E_\mu \geq 10$ GeV, missing $p_T \geq 20$ GeV.

$$e^- p - \rightarrow e^- \mu^+ \nu_\mu X$$



$$e^- p - \rightarrow e^- \mu^+ \nu_\mu X$$

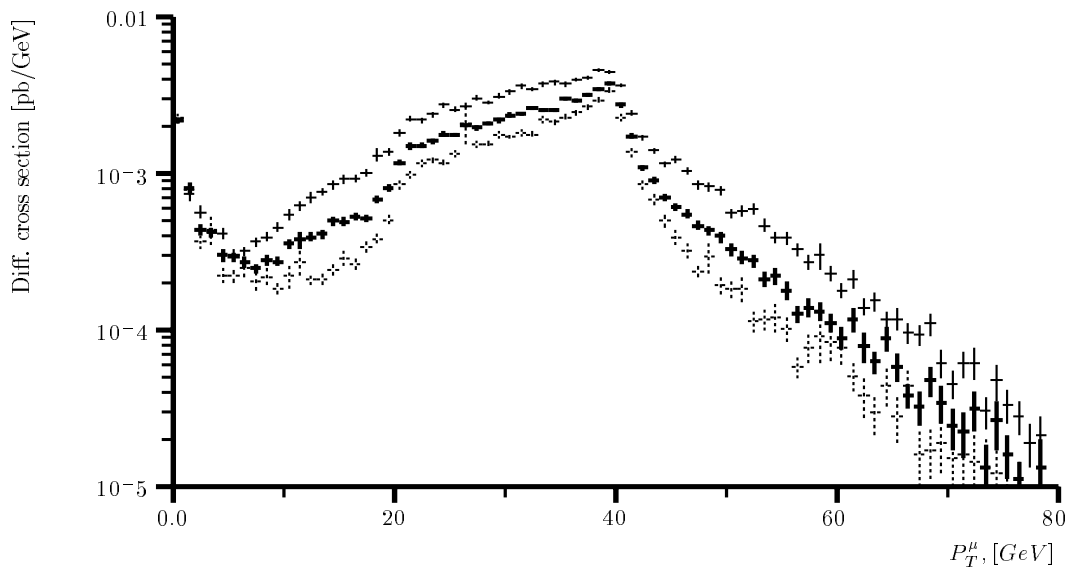
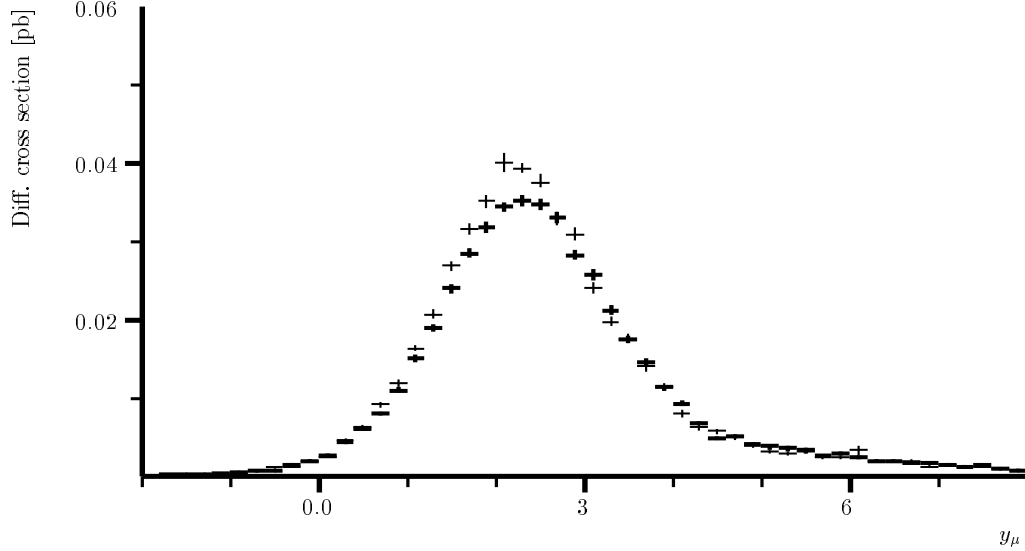


Figure 7: Distribution of muon transverse momentum in the reaction $e^- p \rightarrow e^- \mu^+ \nu_\mu X$. Upper plot: no kinematical cuts, solid lines - standard case, dash lines - anomalous three vector boson couplings case, $\lambda = 0$, $k = 0$, thin solid lines - $\lambda = 0$, $k = 2$. Lower plot: the same distributions after kinematical cuts $E_\mu \geq 10$ GeV, missing $p_T \geq 20$ GeV.

$$e^- p - \rightarrow e^- \mu^+ \nu_\mu X$$



$$e^- p - \rightarrow e^- \mu^+ \nu_\mu X$$

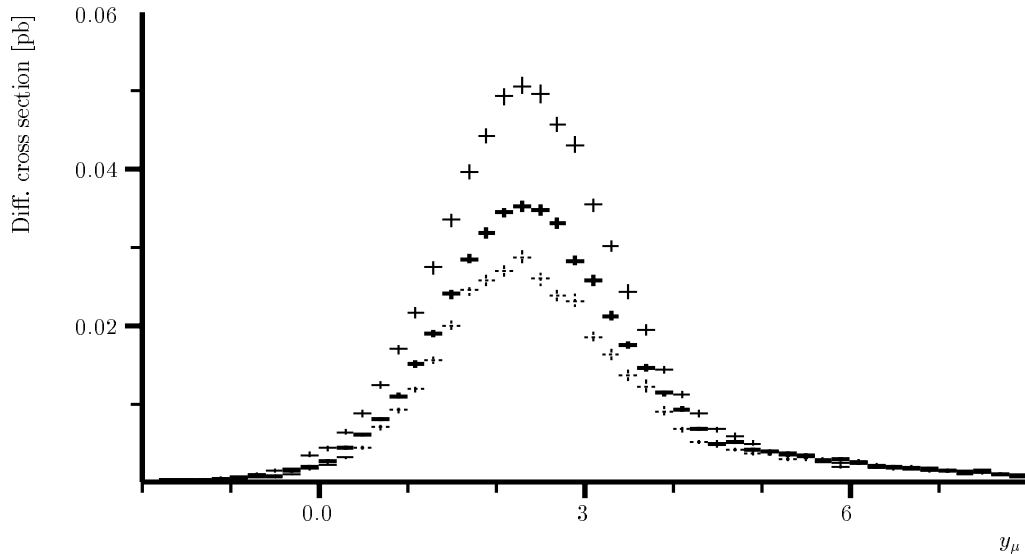


Figure 8: Distribution of muon rapidity in the reaction $e^- p \rightarrow e^- \mu^+ \nu_\mu X$. Upper plot: no kinematical cuts, solid lines - standard case, dash lines - anomalous three vector boson couplings case, $\lambda = 1$, $k = 1$. Lower plot: no kinematical cuts, solid lines - standard case, dash lines - anomalous three vector boson couplings case, $\lambda = 0$, $k = 0$, thin solid lines - $\lambda = 0$, $k = 2$.